

See discussions, stats, and author profiles for this publication at: <https://www.researchgate.net/publication/227708170>

# Liquid Slip on a Nanostructured Surface

ARTICLE *in* LANGMUIR · JUNE 2012

Impact Factor: 4.46 · DOI: 10.1021/la302264t · Source: PubMed

---

CITATIONS

8

---

READS

37

## 5 AUTHORS, INCLUDING:



Doojin Lee

Okinawa Institute of Science and Technology

11 PUBLICATIONS 70 CITATIONS

SEE PROFILE

## Liquid Slip on a Nanostructured Surface

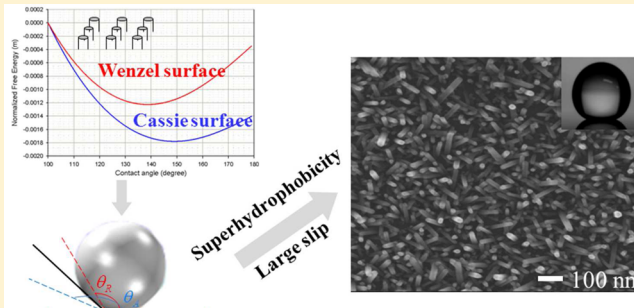
Doo Jin Lee,<sup>†</sup> Ki Yeon Cho,<sup>†</sup> Soohwan Jang,<sup>‡</sup> Young Seok Song,<sup>\*,§</sup> and Jae Ryoun Youn<sup>\*,†</sup>

<sup>†</sup>Research Institute of Advanced Materials (RIAM), Department of Materials Science and Engineering, Seoul National University, Daehak-Dong, Gwanak-Gu, Seoul, 151-744, Korea

<sup>‡</sup>Department of Chemical Engineering and <sup>§</sup>Department of Fiber System Engineering, Dankook University, 126 Jukjeon-dong, Suji-gu, Yongin-si, Gyeonggi-do, 448-701, Korea

### Supporting Information

**ABSTRACT:** We explored a liquid slip, referred to as the Navier slip, at liquid–solid interface. Such a slip is provoked by the physicochemical features of the liquid–solid system. The goal of this study was to investigate the effect of a nanoengineered surface structure on liquid slip by fabricating the self-assembly structure of nano Zinc oxide (*n-ZnO*). We have also examined how the liquid–solid surface interaction controlled by hydrophobic chemical treatment affects the liquid slip. The findings showed that liquid slip increases with decreasing the characteristic length scales (e.g., channel height and depth), resulting in drag reduction. It was also found that dewetted (Cassie) state due to the generation of air gap developed by *n-ZnO* was more critical for the liquid slip than the minimization of interface interaction. The linear and nonlinear Navier slip models showed that liquid slip behavior is more obvious when increasing the nonlinearity. This study will contribute to understanding of the underlying physics behind fluid slip phenomena, such as the Navier slip for Newtonian liquids and Maxwell's slip for Newtonian gases.



### INTRODUCTION

No-slip condition implies that a fluid has zero velocity at a solid boundary.<sup>1</sup> Although the no-slip boundary condition has been widely applied to scientific and engineering problems, liquid slip is also a generally accepted phenomenon that occurs when a viscous fluid moves adjacent to a solid boundary.<sup>2,3</sup> In particular, the slip phenomenon draws big interest as precision systems are fabricated at micrometer or nanometer scale and adopted in a variety of applications such as microfluidics, MEMS, sensors, friction systems, and biophysics.<sup>4,5</sup> For instance, it is reported that extraordinarily fast flow can be generated in nanoscale structures with the help of the slip phenomenon, which would have a wide range of potential applications for transdermal drug and selective chemical sensing in biological channels.<sup>6</sup>

While the liquid slip has been observed experimentally at micro and nanoscale, its fundamental mechanism is still controversial and has yet to be fully understood.<sup>7–11</sup> In general, it is known that liquid molecules are capable of slipping at liquid–solid interface when the liquid possesses a low wettability due to superhydrophobicity, thus resulting in drag reduction. This is the so-called Navier slip for a Newtonian liquid (similarly Maxwell's slip for a Newtonian gas). The Navier slip,  $\mathbf{u}_{\text{slip}}$ , still remains as a gold standard of liquid slip and is expressed as  $\mathbf{u}_{\text{slip}} = \lambda \mathbf{n} \cdot (\nabla \mathbf{u} + \nabla \mathbf{u}^T)$ , where  $\mathbf{n}$  denotes the normal vector to the surface,  $\mathbf{u}$  is the velocity vector, and  $\lambda$  is a constant with the unit of length affected by physicochemical properties of a liquid–solid system.<sup>12</sup> In some cases, the

nonlinear Navier slip law where the slip length is a function of the shear stress is employed, since the simple linear Navier slip law may fail to describe the slip behavior well.<sup>13</sup>

On the other hand, slip flow regimes have been classified by using the Knudsen number, and the classical Navier–Stokes equation has been modified by adding a new velocity concept.<sup>14,15</sup> It has been proven that hydrophobic coating induces an increase in the slip velocity due to minimized surface energy in microchannels.<sup>10</sup> The small slip length in hydrophilic channels and the large slip length in hydrophobic channels have been calculated analytically by using the excessive flow rate of the Poiseuille flow for the applied pressure drop.<sup>16</sup> The findings from nanoscale hydrodynamic experiments and molecular dynamic simulations indicate that the slip length may be gigantic compared with the dimension of the observing system. For example, pressure-driven flow rates through an aligned MWCNT membrane with pores of a 7-nm-diameter are 4 to 5 orders of magnitude higher than those predicted by using the conventional fluid flow.<sup>6,17</sup>

Liquid slip depends on various parameters such as a nonlinear relationship between slip length and local shear rate,<sup>18,19</sup> inherent properties of suspended liquid,<sup>20</sup> fluid–surface interaction,<sup>21–23</sup> and friction reduction by surface structures.<sup>24–28</sup> It has been reported that fluid–solid molecular

Received: June 4, 2012

Revised: June 19, 2012

Published: June 21, 2012

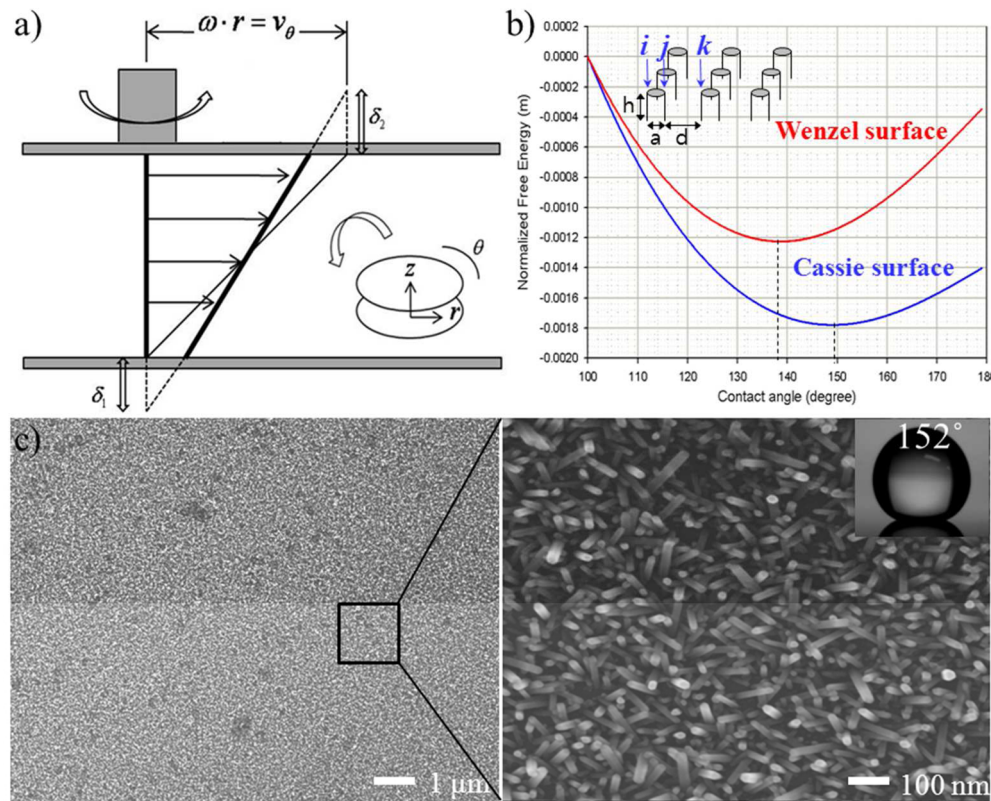


**Figure 1.** (a) Schematic diagram of a parallel-disk rheometer with liquid wall slip at angular velocity ( $\omega$ ) and slip length ( $\delta$ ); (b) normalized Free energy with contact angle of both Wenzel and Cassie surfaces; and (c) SEM image of  $n\text{-ZnO}$  nanostructured surface and magnified view of the  $n\text{-ZnO}$  hexagonal pillars.

interaction has a more critical effect on the slip length than the type of flow.<sup>21</sup> Also, low surface free energy reduces the molecular attraction between liquid and surface.<sup>22</sup> Thermodynamically stable nanostructures have been fabricated to maximize the slip length.<sup>24–28</sup> The liquid–solid contact area was significantly minimized by superhydrophobic nanoturf surface<sup>24</sup> so that air pockets below the liquid could support the flow, resulting in a very large slip length of about 50  $\mu\text{m}$ . A giant slip length as large as 185  $\mu\text{m}$  was achieved by developing almost perfectly structured surfaces<sup>25</sup> with control of the pitch and the height of pillars, which delayed the transition from the dewetted (Cassie) state to the wetted (Wenzel) state under pressurized flow conditions. The scaling law approach was also employed for generic geometries to predict the effective slip length and to quantify their superlubricating potential.<sup>26</sup> Large slip effects may be interpreted by considering the contact angle (CA) according to the dewetting behavior between fluid and solid surfaces.<sup>27,28</sup>

Liquid slip, indeed, is an important phenomenon occurring especially at micro and nanoscale, which requires the in-depth understanding on the underlying physics and chemistry. In this study, the liquid slip behavior is analyzed quantitatively with respect to surface interaction and surface structure. The linear and nonlinear slip laws are considered to investigate the liquid slip behavior. Our results suggest that liquid slip is affected more greatly by the characteristic length scale (e.g., channel depth and height) and the superhydrophobicity induced by a nanostructure than by the liquid–solid interaction.

**Theoretical Background.** Figure 1a shows a rheometric measurement system with two parallel disks, where the upper disk rotates at an angular velocity of  $\omega$ . The fine and bold lines

are the velocity distributions without and with wall slip, respectively. When the upper disk rotates at a velocity of  $\omega \cdot r$  where  $r$  is the radius, the fluid velocity adjacent to the upper disk decreases due to the slip at the wall. Assuming steady, laminar, and isothermal flow, the momentum balance of the fluid is expressed in the cylindrical coordinate system as follows (body force and cylindrical edge effect are neglected):

$$\frac{\partial \tau_{\theta z}}{\partial z} = 0 \quad (1)$$

For the slip system shown in Figure 1a, boundary conditions are given by the following equations:

$$v_\theta(z=0) = \delta_1 \left( \frac{\partial v_\theta}{\partial z} \right)^m \quad (2)$$

$$v_\theta(z=h) = \omega \cdot r - \delta_2 \left( \frac{\partial v_\theta}{\partial z} \right)^m$$

where  $h$  is the gap between the two disks,  $v_\theta$  is the velocity in  $\theta$  direction, and  $\delta_1$  and  $\delta_2$  are the slip lengths over the lower disk and upper disk, respectively. The two slip lengths are assumed equal for simplicity. The exponent  $m$  stands for the nonlinearity of the slip law. The linear Navier slip law is considered when the exponent is equal to unity. Then, the momentum balance and boundary condition reduce to the following two universal forms:

$$v_\theta(r, z) = C_1(z + \delta C_1^{m-1}) \quad (3)$$

$$C_1^m + (h/2\delta)C_1 - (\omega \cdot r / 2\delta) = 0 \quad (4)$$

The rotational torque ( $T$ ) is derived as below:

$$T = \int_0^R (2\pi r^2 \tau_{\theta z}) dr = 2\pi\mu \int_0^R r^2 C_1 dr \quad (5)$$

The rotational torque is simply derived for the linear Navier slip model. On the other hand, the nonlinear Navier slip models show numerically solvable semianalytical equations. For the linear Navier slip model, the following analytical equation is obtained:

$$h + 2\delta = \pi \frac{\mu\omega}{2T} R^4 \quad (6)$$

The torque applied to the rotating disk is measured in a range of various shear rates and angular frequencies. At each shear rate and angular velocity, the torque is recorded after the rotating disk reaches steady state with less than 3% deviation. The slip lengths are calculated using the angular velocity, measured torque, and measured viscosity.

The  $n\text{-ZnO}$  surface prepared in this study yields either the noncomposite Wenzel state or the composite Cassie state.<sup>29</sup> The free energy of a surface determines whether the states show sticky or slippery condition. The energy, which is primarily governed by the surface geometry, is calculated by coupling geometrical constitution with free energy transition.<sup>30</sup> For the noncomposite state, the thermodynamic expressions are

$$\theta_i \frac{L_i^2}{\sin^2 \theta_i} - L_i^2 \cot \theta_i = \theta_j \frac{L_j^2}{\sin^2 \theta_j} - L_j^2 \cot \theta_j \quad (7)$$

$$F_{i \rightarrow j}/\gamma^{la} = \left( \theta_j \frac{L_j}{\sin \theta_j} - \theta_i \frac{L_i}{\sin \theta_i} \right) + a \cos \theta_Y \quad (8)$$

$$\theta_j \frac{L_j^2}{\sin^2 \theta_j} - L_j^2 \cot \theta_j + 2bh = \theta_k \frac{L_k^2}{\sin^2 \theta_k} - L_k^2 \cot \theta_k \quad (9)$$

$$F_{j \rightarrow k}/\gamma^{la} = \left( \theta_j \frac{L_j}{\sin \theta_j} - \theta_k \frac{L_k}{\sin \theta_k} \right) - (b + 2h) \cos \theta_Y \quad (10)$$

For the composite state, the terms,  $2bh$  in eq 9 and  $2h \cos \theta_Y$  in eq 10 showing the effect of the pillar height vanish, and  $-b$  in eq 10 becomes  $+b$ . In our case,  $a$  and  $h$  are the width and height of the  $n\text{-ZnO}$  pillar, and  $d$  is the spacing between two pillars. The values of width, height, and spacing are 20 nm, 200 nm, and 100 nm, respectively. Equations 7 and 9 are derived by considering the geometrical constitution of the  $n\text{-ZnO}$  surface. When the edge of the meniscus of a droplet moves from position  $i$  to  $j$ , the difference in free energy (FE) is given by eq 8. The two FEs at each position are represented by surface tension and arc-length of the meniscus by using  $F_i = \gamma^{la} l_i^{la} + \gamma^{ls} l_i^{ls} + C$  and  $F_j = \gamma^{la} l_j^{la} + \gamma^{sa} l_j^{sa} + C$ , where  $C$  is the FE of the portion that remains unchanged. The FE difference from position  $j$  to  $k$  is also expressed as eq 10 by using  $F_j = \gamma^{la} l_j^{la} + \gamma^{ls} l_j^{ls} + C$  and  $F_k = \gamma^{la} l_k^{la} + \gamma^{sa} l_k^{sa} + C$ . Equations 8 and 10 were used repeatedly to calculate the FE barriers and the equilibrated contact angles of the Wenzel and Cassie states. The imposed initial condition is that the contact angle of the flat  $\text{ZnO}$  surface<sup>31</sup> is 100° and the diameter of the droplet is 10<sup>-2</sup> m. The normalized free energy shows that the Wenzel surface and the Cassie surface have the

minimum free energies at angles of 138° and 149° (Figure 1b). These theoretical results imply that the  $n\text{-ZnO}$  surface with a contact angle of 152° is the Cassie surface.

## EXPERIMENTAL SECTION

Silicone oil with a viscosity of 1 Pa·s was employed to measure wall slip over smooth, hydrophobic, and  $n\text{-ZnO}$  nanostructured surfaces. Rheological properties of the fluid were measured with a parallel disk rheometer (AR-2000, TA Instrument, U.S.A.).

For a smooth surface, a steel disk was finely polished to minimize surface roughness. For a hydrophobic surface, Trichloro (1H,1H,2H,2H-perfluoroctyl) silane was spin-coated onto the smooth surface.  $n\text{-ZnO}$  nanostructure was constructed onto a glass substrate by the self-assembling method<sup>32</sup> in a bid to generate superhydrophobicity. To grow the  $n\text{-ZnO}$  on the glass, the glass substrate was washed in a cleaning solution ( $\text{H}_2\text{SO}_4/\text{H}_2\text{O}_2 = 4:1$ ) at 110 °C for 15 min and then deionized with water for 5 min.  $\text{ZnO}$  nuclei were created by using 30 mM zinc acetate [ $\text{Zn}(\text{C}_2\text{H}_3\text{O}_2)_2$ ] solution in ethanol at 90 °C for 15 min. The seed solution was spin-coated onto the glass substrate at 1500 rpm for 60 s. After then, the seed coated substrates were thermally annealed at 100 °C for 5 min to remove the residual solvent. The glass substrates were immersed in an aqueous solution consisting of 25 mM zinc nitrate hexahydrate [ $\text{Zn}(\text{NO}_3)_2 \cdot 6\text{H}_2\text{O}$ ], 25 mM hexamethylenetetramine [ $\text{C}_6\text{H}_{12}\text{N}_4$ ] (HMT), and deionized (DI) water. The growth of  $\text{ZnO}$  nanopillars was carried out at 90 °C for 60 min.

The gaps between two disks of the rheometer were varied to 1000, 500, 200, 100, 80, 60, and 40 μm to investigate the scale dependency of the liquid slip behavior. Experimental data on the rotating velocity, torque, and viscosity were acquired in a steady shear rate mode at the angular velocity ranging from 0.1 to 300 rad/s. Oscillatory experiments were also carried out to verify the drag reduction in the steady shear rate mode (see Supporting Information Figure S1).

## RESULTS AND DISCUSSION

Surface properties strongly affect flow resistance through a channel, especially microchannels or nanochannels with a large surface-to-volume ratio. Surface friction may be decreased as the corresponding surface roughness is increased, which is contrary to the common knowledge.<sup>33</sup> Several possible reasons have been suggested for such a reduction of the surface friction, e.g., molecular slip<sup>7</sup> at the solid–liquid interface due to the low interaction energy and the existence of nanobubbles<sup>9–11</sup> at the solid–liquid interface. Micro and nanoengineered structures are of great importance for fabrication of a fluidic device that maintains the dewetted (Cassie) state (i.e., air penetration is impeded). These structures enable very large effective liquid slip.<sup>24</sup> In this study, an  $n\text{-ZnO}$  nanostructure was self-assembled on the glass substrate to generate the dewetted state during steady and oscillatory motion (Figure 1c). It is shown in Figure 1c that the  $n\text{-ZnO}$  pillars were uniformly grown over the entire surface. The  $n\text{-ZnO}$  nanostructure consisting of 20-nm-diameter hexagonal pillars created an air-trapping system, in which liquid could not penetrate readily into the interspace between pillars.<sup>34</sup> Choi and Kim<sup>24</sup> suggested the critical pitch and height of the uniform structure from the calculation of geometrical constitution such that the pitch should be less than 1 μm and the height should be larger than 0.2 μm. Since the liquid is silicone oil ( $\sigma \approx 0.02 \text{ N/m}$ ) and  $\Delta P$  is assumed to be 0.1 MPa (~1 atm) in this study, the critical pitch and height are around 0.3 μm and 55 nm, respectively, which are suitable for the Cassie state of the  $n\text{-ZnO}$  nanostructure. The pillars have very narrow pitches and an average height of 200 nm, which satisfy the dewetted (Cassie) surface condition.<sup>24</sup>

Effective shear stress is obtained from the measured torque and plotted with respect to the shear rate as shown in Figure 2.

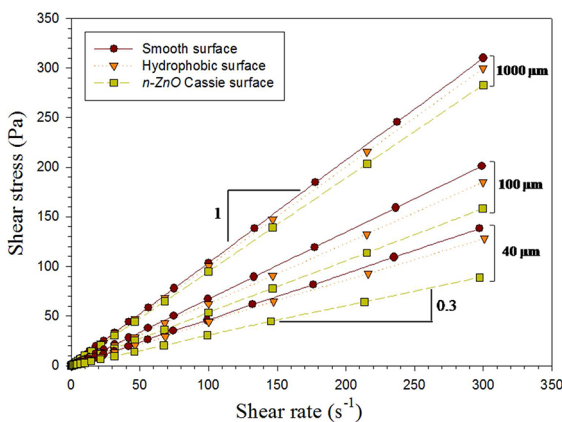


**Figure 2.** Shear stress as a function of shear rate measured for different surfaces.

When the channel height is 1000  $\mu\text{m}$ , the slope of the curve for the smooth surface shows the dynamic viscosity of silicone oil ( $\sim 1 \text{ Pa}\cdot\text{s}$ ) in that the employed liquid is a Newtonian fluid following the relationship of  $\tau = \mu\dot{\gamma}$  (where  $\mu$  is the dynamic viscosity, and  $\dot{\gamma}$  is the shear rate). In this case, the viscosity does not show any dependency on the shear rate, temperature and pressure which are dependent variables for the Non-Newtonian viscosity models such as Cross-WLF model, power-law model, Carreau model, and so forth. The slope decreases with decreasing the channel height from 1000 to 40  $\mu\text{m}$  (Figure 2 and SI Figure 2). During the steady shear experiments, dynamic viscosities for the smooth, hydrophobic, and *n*-ZnO Cassie surfaces decrease significantly with respect to the channel height (Figure 3a–c and SI Figure 1). It shows that the liquid slip is clearly dependent on the characteristic length scale. For the *n*-ZnO nanostructured surface, the viscosity decreasing rate is larger than that of the smooth surface or the hydrophobic surface, which can be explained by the reduction of solid–liquid friction due to trapped air in the dewetted (Cassie) state.

The linear relationship between slip velocity and shear rate at the wall known as the linear Navier slip law is invited often to bridge between theory and experimental data. In some cases, the nonlinear Navier slip law can provide better results for describing the slip phenomenon.<sup>13,18</sup> In our case, the liquid slip is increased with the nonlinearity as shown in Figure 4a. Interestingly, the slip is also increased when the channel height is decreased (see the inset in the figure). Figure 4b obviously demonstrates that the constant  $C_1$  (meaning shear rate at the wall) drastically decreases with the nonlinearity at the same slip length.

When the channel height is 40  $\mu\text{m}$ , the dynamic viscosity and liquid slip length of the smooth surface are largely different from those of the hydrophobic or *n*-ZnO Cassie surfaces (Figure 5a,b). When the surface is coated with a hydrophobic solution, the liquid–solid surface interaction is decreased because the low free surface energy reduces the molecular attraction between the liquid and the surface, resulting in a larger slip length than that of the smooth surface. In the case of the *n*-ZnO nanostructure, the air cushions below the liquid act as frictionless surfaces such that the lower dynamic viscosity and the largest liquid slip ( $\sim 47 \mu\text{m}$ ) are obtained. A nonlinear relationship exists between the amount of slip and the local

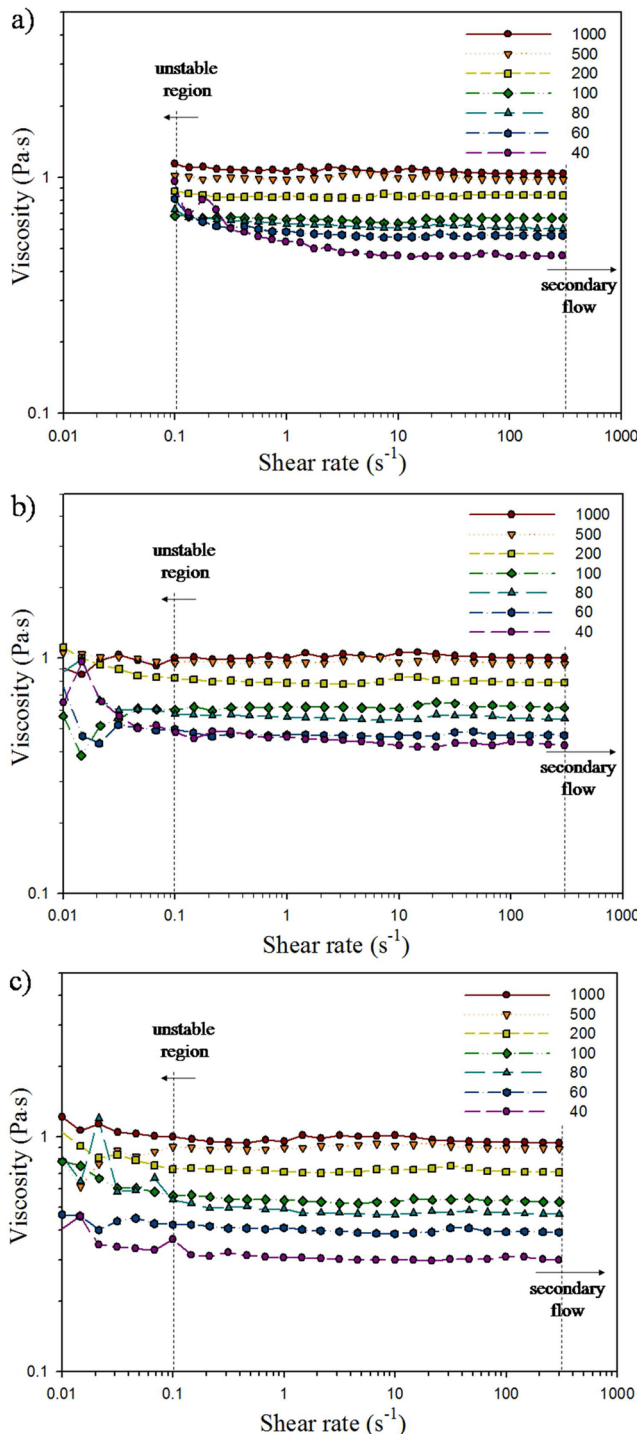


**Figure 3.** Dynamic viscosity measured by the steady shear experiment for various channel heights: (a) smooth surface, (b) hydrophobic surface, and (c) *n*-ZnO Cassie surface.

shear rate (Figure 5b), which is not explained by the linear Navier slip model. By using molecular dynamics,<sup>18</sup> Peter et al. claimed that the boundary condition may be nonlinear even though the liquid is still Newtonian.

Liquid slip can have more important role when the characteristic length is scaled down. For example, flow rates through a slippery channel are up to 4 to 5 orders of magnitude higher than flow rates through pores of 7-nm-diameter MWCNTs<sup>6</sup> since the characteristic length scale of the system

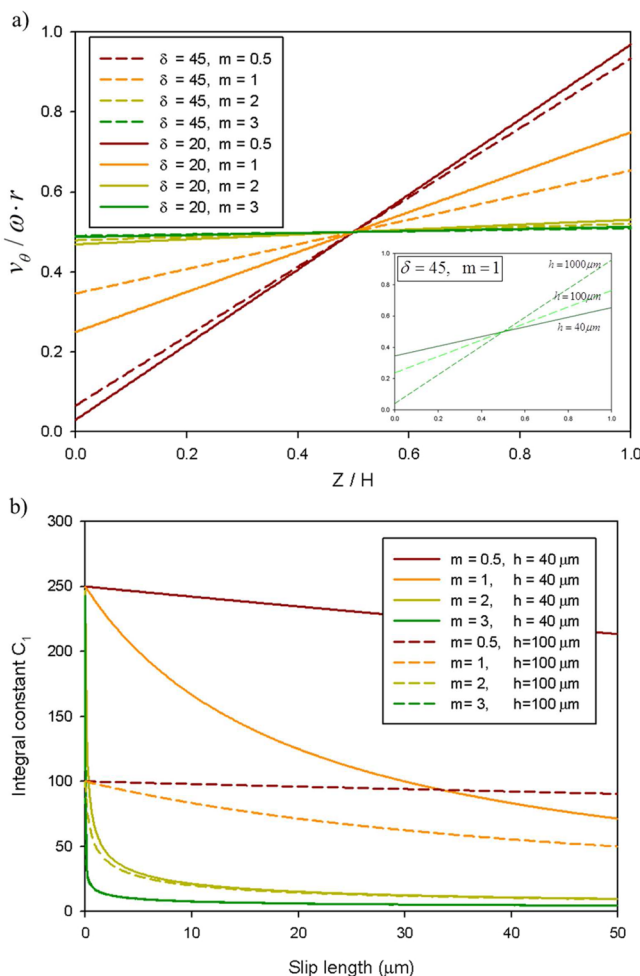


**Figure 4.** (a) Velocity profiles with the linear and nonlinear Navier slip exponents. An inset graph shows a height dependence on slip velocity, (b) integral constant  $C_1$  and slip length with the linear and nonlinear Navier slip exponents.

is extremely small. In this sense, the liquid slip length needs to be described in terms of the characteristic length to figure out the slip effect from a more quantitative standpoint (Figure 6). All three surfaces showed significant increase in the slip length as the height was scaled down. Among them, the  $n\text{-ZnO}$  nanostructure surface showed the largest increase in the slip length. When the liquid–solid interaction becomes large, the CA decreases due to the larger surface area between the liquid and the solid. Adhesion is expressed thermodynamically as  $W_{\text{SL}} = \gamma_{\text{LV}} (1 + \cos \theta)$ , where  $W_{\text{SL}}$  is the work of adhesion and  $\gamma_{\text{LV}}$  is the surface tension of the liquid. In the partial wetting condition, i.e., when  $\gamma_{\text{LS}} + \gamma_{\text{LV}} > \gamma_{\text{SV}}$ , the boundary conditions are very different from the no-slip condition.<sup>28</sup> The liquid slip length can increase significantly as the CA increases. Our experimental results are in good agreement with the above explanation, i.e., the liquid slip length increases with the CA. For the  $n\text{-ZnO}$  nanostructure with a CA of  $152^\circ$ , the slip length is larger than those of the hydrophobic and smooth surfaces with relatively low CAs for every channel height. The effect of the slip length on drag reduction can be demonstrated simply as  $(\tau_{\text{slip}}/\tau_{\text{no-slip}}) = 1/(1 + \delta/h)$ , where  $\tau_{\text{slip}}$  and  $\tau_{\text{no-slip}}$  are the shear stresses at the wall when slip and no-slip boundary conditions are applied, respectively.<sup>24</sup> When  $h/H = 0.04$  ( $40 \mu\text{m}$  in height at the shortest in our case), the value of  $\delta/h$  is 1.2,

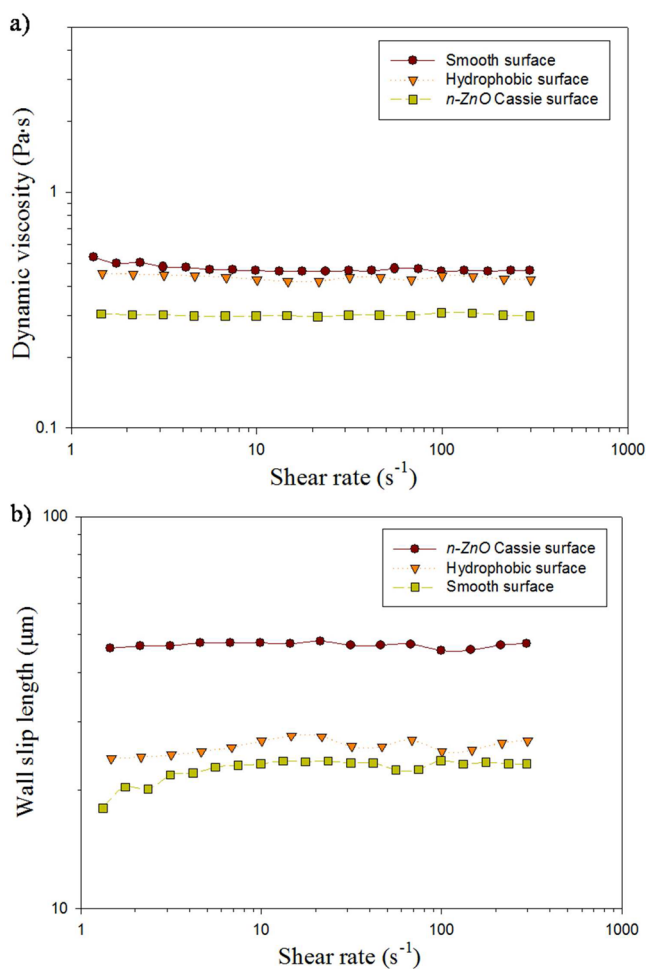


**Figure 5.** (a) Dynamic viscosity and (b) wall slip length measured by the steady shear experiment at  $40 \mu\text{m}$  channel height for smooth, hydrophobic, and  $n\text{-ZnO}$  Cassie surfaces.

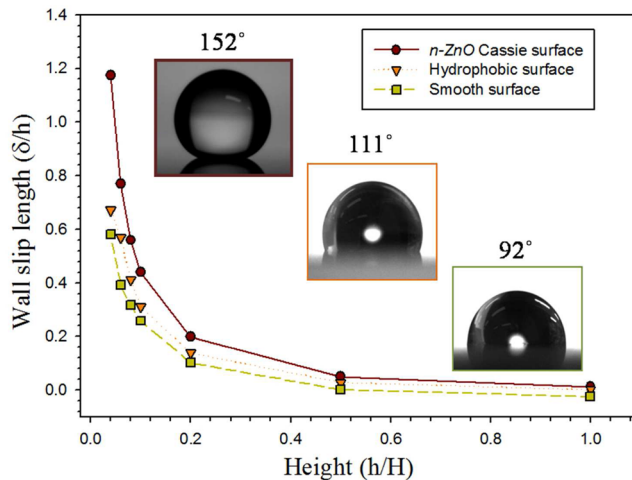


**Figure 6.** Wall slip length measured with respect to the channel height for different surface features.

which represents nearly 55% reduction of the drag compared with the shear stress in no-slip condition. This result implies that much higher liquid transport is possible at micro and nanoscales.

It is noticed that the liquid slip is affected significantly by the characteristic length scale and that a large liquid slip results from superhydrophobicity, which is induced by the nanostructure rather than by the minimization of liquid–solid interaction. It is expected that this study will be able to provide meaningful insight into microfluidics and micro and nanoplates, particularly when small driving power or energy is required to operate such fluidic systems.

## CONCLUSION

The influence of liquid–solid surface interaction and nano-engineered surface structure on liquid slip was investigated. It was found that the nanostructure fabricated for the dewetted (Cassie) state had more effect on the liquid slip than the minimization of the liquid–solid surface interaction. The results revealed that the molecular slip or nanobubbles generated by interaction minimization were not good enough to provoke large slip and that the Cassie surface should be guaranteed for the large slip. Drag reduction was also increased significantly as the characteristic length was scaled down to micro and nanoscale. The linear and nonlinear Navier slip models showed that liquid slip behavior is more obvious when increasing the nonlinearity. The large liquid slip can be utilized to transform conventional micro and nanofluidic platforms into highly energy efficient devices with higher transport capability and less driving energy.

## ASSOCIATED CONTENT

### Supporting Information

Oscillatory data of storage modulus, loss modulus, and complex viscosity in frequency sweep modes with smooth, hydrophobic, and *n*-ZnO Cassie surfaces; shear stress versus shear rate with respect to the channel height. This material is available free of charge via the Internet at <http://pubs.acs.org>.

## AUTHOR INFORMATION

### Corresponding Author

\*Young Seok Song: Tel. +82-31-8005-3567; Fax +82-31-8005-2209; E-mail [ysong@dankook.ac.kr](mailto:ysong@dankook.ac.kr). Jae Ryoun Youn: Tel. +82-2-880-8326; Fax +82-2-885-9671; E-mail [jaeryoun@snu.ac.kr](mailto:jaeryoun@snu.ac.kr).

### Notes

The authors declare no competing financial interest.

## ACKNOWLEDGMENTS

This study was supported by Basic Science Research Program through the National Research Foundation of Korea (NRF) funded by the Ministry of Education, Science and Technology (2010-0006337). Also, this study was supported by the Korea Science and Engineering Foundation (KOSEF) grant funded by the Korean government (MEST) (R11-2005-065) through the Intelligent Textile System Research Center (ITRC). The authors are grateful for the support.

## REFERENCES

- (1) White, F. M. *Viscous fluid flow*; McGraw-Hill: New York, 1991.
- (2) Rothstein, J. P. Slip on superhydrophobic surfaces. *Annu. Rev. Fluid Mech.* **2010**, *42*, 89–109.
- (3) Migler, K. B.; Hervet, H.; Leger, L. Slip transition of a polymer melt under shear stress. *Phys. Rev. Lett.* **1993**, *70*, 287–290.
- (4) Zhu, Y.; Granick, S. Rate-dependent slip of Newtonian liquid at smooth surfaces. *Phys. Rev. Lett.* **2001**, *87*, 096105–1–3.
- (5) Sbragaglia, M.; Prosperetti, A. A note on the effective slip properties for microchannel flows with ultrahydrophobic surfaces. *Phys. Fluids* **2007**, *19*, 043603–1–8.
- (6) Majumder, M.; Chopra, N.; Andrews, R.; Hinds, B. J. Nanoscale hydrodynamics - Enhanced flow in carbon nanotubes. *Nature* **2005**, *438* (7064), 44–44.
- (7) Blake, T. D. Slip between a Liquid and a Solid - Tolstoi, D.M. (1952) Theory Reconsidered. *Colloids Surf.* **1990**, *47*, 135–145.
- (8) Cho, J. H. J.; Law, B. M.; Rieutord, F. Dipole-dependent slip of Newtonian liquids at smooth solid hydrophobic surfaces. *Phys. Rev. Lett.* **2004**, *92*, (16).
- (9) Ruckenstein, E.; Rajora, P. On the No-Slip Boundary-Condition of Hydrodynamics. *J. Colloid Interface Sci.* **1983**, *96* (2), 488–491.
- (10) Tretheway, D. C.; Meinhart, C. D. Apparent fluid slip at hydrophobic microchannel walls. *Phys. Fluids* **2002**, *14* (3), L9–L12.
- (11) de Gennes, P. G. On fluid/wall slippage. *Langmuir* **2002**, *18* (9), 3413–3414.
- (12) Alexeyev, A. A.; Vinogradova, O. I. Flow of a liquid in a nonuniformly hydrophobized capillary. *Colloids Surf., A* **1996**, *108*, 173–179.
- (13) Schowalter, W. R. The Behavior of Complex Fluids at Solid Boundaries. *J. Non-Newtonian Fluid Mech.* **1988**, *29* (1–3), 25–36.
- (14) Dongari, N.; Sharma, A.; Durst, F. Pressure-driven diffusive gas flows in micro-channels: from the Knudsen to the continuum regimes. *Microfluid Nanofluid* **2009**, *6*, 679–692.
- (15) Brenner, H. Fluid mechanics revisited. *Physica A* **2006**, *370*, 190–224.
- (16) Choi, C. H.; Westin, K. J. A.; Breuer, K. S. Apparent slip flows in hydrophilic and hydrophobic microchannels. *Phys. Fluids* **2003**, *15* (10), 2897–2902.
- (17) Whiby, M.; Cagnon, L.; Thanou, M.; Quirke, N. Enhanced fluid flow through nanoscale carbon pipes. *Nano Lett.* **2008**, *8* (9), 2632–2637.
- (18) Thompson, P. A.; Troian, S. M. A general boundary condition for liquid flow at solid surfaces. *Nature* **1997**, *389* (6649), 360–362.
- (19) Laun, H. M.; Rady, M.; Hassager, O. Analytical solutions for squeeze flow with partial wall slip. *J. Non-Newtonian Fluid Mech.* **1999**, *81* (1–2), 1–15.
- (20) Yang, S. P.; Zhu, K. Q. Analytical solutions for squeeze flow of Bingham fluid with Navier slip condition. *J. Non-Newtonian Fluid Mech.* **2006**, *138* (2–3), 173–180.
- (21) Cieplak, M.; Koplik, J.; Banavar, J. R. Boundary conditions at a fluid-solid interface. *Phys. Rev. Lett.* **2001**, *86* (5), 803–806.
- (22) Pit, R.; Hervet, H.; Leger, L. Direct experimental evidence of slip in hexadecane: Solid interfaces. *Phys. Rev. Lett.* **2000**, *85* (5), 980–983.
- (23) Watanabe, K.; Yanuar; Udagawa, H. Drag reduction of Newtonian fluid in a circular pipe with a highly water-repellent wall. *J. Fluid Mech.* **1999**, *381*, 225–238.
- (24) Choi, C. H.; Kim, C. J. Large slip of aqueous liquid flow over a nanoengineered superhydrophobic surface. *Phys. Rev. Lett.* **2006**, *96*, (6).
- (25) Lee, C.; Choi, C. H.; Kim, C. J. Structured surfaces for a giant liquid slip. *Phys. Rev. Lett.* **2008**, *101*, (6).
- (26) Ybert, C.; Barentin, C.; Cottin-Bizonne, C.; Joseph, P.; Bocquet, L. Achieving large slip with superhydrophobic surfaces: Scaling laws for generic geometries. *Phys. Fluids* **2007**, *19*, (12).
- (27) Baudry, J.; Charlaix, E.; Tonck, A.; Mazoyer, D. Experimental evidence for a large slip effect at a nonwetting fluid-solid interface. *Langmuir* **2001**, *17* (17), 5232–5236.
- (28) Barrat, J. L.; Bocquet, L. Large slip effect at a nonwetting fluid-solid interface. *Phys. Rev. Lett.* **1999**, *82* (23), 4671–4674.
- (29) Shirtcliffe, N. J.; McHale, G.; Newton, M. I.; Chabrol, G.; Perry, C. C. Dual-scale roughness produces unusually water-repellent surfaces. *Adv. Mater.* **2004**, *16* (21), 1929–1932.
- (30) Li, W.; Amirfazli, A. A thermodynamic approach for determining the contact angle hysteresis for superhydrophobic surfaces. *J. Colloid Interface Sci.* **2005**, *292* (1), 195–201.

- (31) Han, J.; Gao, W. Surface Wettability of Nanostructured Zinc Oxide Films. *J. Electron. Mater.* **2009**, *38* (4), 601–608.
- (32) Vayssières, L. Growth of arrayed nanorods and nanowires of ZnO from aqueous solutions. *Adv. Mater.* **2003**, *15* (5), 464–466.
- (33) Cottin-Bizonne, C.; Barrat, J. L.; Bocquet, L.; Charlaix, E. Low-friction flows of liquid at nanopatterned interfaces. *Nat. Mater.* **2003**, *2* (4), 237–240.
- (34) Marmur, A. Wetting on hydrophobic rough surfaces: To be heterogeneous or not to be? *Langmuir* **2003**, *19* (20), 8343–8348.